

Safe and Smooth: Certified Continuous-Time Range-Only Localization

Frederike Dümbgen Connor Holmes Timothy D. Barfoot

Abstract—A common approach to localize a mobile robot is by measuring distances to points of known positions, called anchors. Locating a device from distance measurements is typically posed as a non-convex optimization problem, stemming from the nonlinearity of the measurement model. Non-convex optimization problems may yield suboptimal solutions when local iterative solvers such as Gauss-Newton are employed. In this paper, we design an optimality certificate for continuous-time range-only localization. Our formulation allows for the integration of a motion prior, which ensures smoothness of the solution and is crucial for localizing from only a few distance measurements. The proposed certificate comes at little additional cost since it has the same complexity as the sparse local solver itself: linear in the number of positions. We show, both in simulation and on real-world datasets, that the efficient local solver often finds the globally optimal solution (confirmed by our certificate), but it may converge to local solutions with high errors, which our certificate correctly detects.

Index Terms—Optimization and optimal control, localization, certifiable algorithms, global optimality, Lagrangian duality

I. INTRODUCTION

Localizing a moving robot is an essential component of many real-world applications. One common approach to localization, in particular when global positioning system (GPS) or cameras are unavailable, is to measure the distances to a certain number of fixed points, called anchors or beacons. In mobile indoor localization, for instance, a phone can be localized by inferring distances to WiFi access points from the time of flight or received signal strength of emitted pulses [1]. As another example, designated anchors equipped with the ultra-wideband (UWB) technology may be used, for instance, for autonomous lawnmowers operating in environments where feature-based computer vision methods are compromised [2], or for drones flying in GPS-denied areas [3]. Finally, in marine robotics, a common localization strategy for autonomous submarines is to emit sonar pulses and measure the time of flight to stationary beacons [4]. In all these examples, the locations of the anchors are known a priori, or can be estimated in a separate procedure [5]. The remaining task is to determine a moving device’s trajectory based on distance measurements, which is also known as multilateration.

Although multilateration has been studied for a long time, many important open questions persist. For instance, when approached from a robotics point of view, multilateration is

This work was funded in part by the Swiss National Science Foundation, Postdoc Mobility under Grant 206954 and in part by the Natural Sciences and Engineering Research Council of Canada (NSERC).

The authors are with the University of Toronto Robotics Institute, University of Toronto, Toronto, M5S 1A4, Canada. Corresponding author: Frederike Dümbgen (frederike.dumbgen@utoronto.ca).

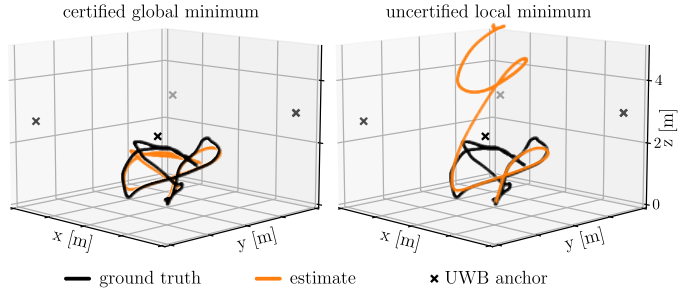


Fig. 1: A flying drone measures distances to fixed anchor points in an arena. The two solutions are obtained by running a continuous-time range-only localization scheme from two different initializations. We propose an efficient optimality certificate based on Lagrangian duality that correctly identifies the left solution as the global minimum.

called range-only localization and typically involves solving a nonlinear least-squares optimization problem with, at best, local convergence guarantees [6]. A more optimal approach to multilateration is to exploit principles from distance geometry [7]. However, optimality and recovery guarantees obtained this way usually assume no noise [8], or that each position can be uniquely localized [9], [10]. Figure 1 displays the limitation of these existing methods. In the shown example, a drone is localized based on distance measurements to fixed UWB anchors. The distance measurements are noisy and sparse (we only measure one distance at a time), which rules out optimal solvers from distance geometry [9], [10]. Instead, we can employ a continuous-time range-only localization framework with a local solver [11]. However, as the example shows, such a method may yield a suboptimal solution far from the global optimum, if poorly initialized.

The method presented in this paper allows us to efficiently identify optimal solutions. We first derive a certificate for discrete-time range-only localization without between-point dependencies, which can be used when we measure enough distances at each time. By incorporating smoothness priors, we extend the operating conditions of both solver and certificate to cases where only a few distance measurements are available at each time. This is allowed by posing the problem as continuous-time range-only localization, for which no optimal solvers are known to this date. In the continuous-time framework, smoothness priors are enforced by regularization terms that stem from Gaussian process (GP) regression and allow us to incorporate physical assumptions about the trajectory. As a welcome side effect, the continuous model can be used to interpolate the trajectory, or to obtain closed-form estimates of quantities of interest such as the instantaneous velocity [12]. The proposed certificates show that local solvers

yield the optimal solution in the vast majority of cases. More specifically, the contributions of this paper are:

- certificates for multilateration and range-only continuous-time localization,
- a detailed treatment of how to exploit sparsity to compute the certificates in linear complexity, and
- validation of the proposed certificates, including evaluation on real-world datasets.

This paper is organized as follows. After reviewing related work in Section II, we introduce the certificate for multilateration and continuous-time range-only localization in Sections III-B and III-C, respectively. We include a discussion of our local solver in Section III-D and the certificate computation in Section III-E. We evaluate the certificates in simulation and on a UWB-based drone localization dataset in Section IV, and conclude in Section V.

II. RELATED WORK

Range-only localization The underdetermined nature of distance measurements makes range-only localization a challenging subclass of state estimation problems. When the anchors are unknown and to be estimated along with the moving device, we refer to this as range-only simultaneous localization and mapping (SLAM). To account for the multimodal distribution stemming from underdetermined measurements, prior work has focused on using Gaussian mixture models [13], [14] or sample-based models [15], [16] to approximate the position distribution in a filtering-inspired framework. More accurate than filters are batch solutions, which typically provide the maximum a posteriori (MAP) estimate of the trajectory given all measurements within a given time window [11]. In general, batch solutions are more expensive than filtering, but the sparsity of the underlying measurement graph typically allows for efficient and incremental sparse solvers [17], [18]. In both batch and filter approaches, continuous-time rather than discrete-time trajectory models have been explored [11], through which smoothness can be incorporated, thereby helping with underdetermined measurements. To make the continuous-time estimation tractable, some prior work uses parametric representations with carefully chosen temporal basis functions [19], [20]. A popular alternative is non-parametric GP regression, which is easier to tune and has an elegant connection with physically plausible motion priors [12].

Whatever representation is used, at the core of batch MAP estimation is the solution of a non-convex minimization problem [11]. The latter is most commonly solved with an iterative minimizer, which usually converges to a stationary point, but not necessarily to the global minimum [6]. Different approaches originated in the sensor network localization literature and study semi-definite relaxations and optimality guarantees [21], [22]. However, optimality guarantees only exist for the noiseless case [8], and this approach scales poorly with batch size. Similarly, works inspired by distance geometry (see [7], [23] for overviews of the topic) can be exploited but, again, efficient algorithms with recovery guarantees do not allow for noisy [8] or under-determined problems [9], [10].

With the proposed solution, we can be both efficient and optimal: we use a continuous-time batch approach, but exploit sparsity to keep the cost low enough for online inference, both in solving and certifying the solution. We place no assumptions on noise or uniqueness of the solution – as long as the certificate holds, the solution is optimal.

Optimality certificates In the last 10 years, significant progress was made in certifying solutions of common optimization problems in robotics and related fields. Certificates typically originate from Lagrangian duality principles [24], and were primarily introduced to robotics and computer vision for the problems of pose-graph optimization [25], [26] and rotation averaging [27], respectively. The main difficulty of these problems stems from the non-convex constraints that emerge when estimating rotations. Existing provably optimal solvers require the solution of a semidefinite program (SDP), which extends poorly to large batch sizes. Instead, follow-up works have investigated careful reformulation [28], Riemannian optimization [29], block coordinate descent [30], and an adaptation of, for instance, Gauss-Newton (GN) [31], to speed up the certified solvers. In parallel strands of research, significant progress has been made on using outlier-robust cost functions for optimal line fitting [32] and optimal point-cloud alignment [33], [34], respectively. Very recently, the above ideas have been applied to the joint localization of static points from their inter-point distances [35], [36]. Instead, we consider the widespread anchor-based localization. Furthermore, our method allows for the use of motion priors, crucial for localization in real-world settings where distance measurements may be sparse and corrupted by high noise.

III. METHOD

A. Preliminaries

Our goal is to solve for an unknown state vector over time, which we denote by $\theta(t) \in \mathbb{R}^K$ at time t . The state typically contains the robots' position $x(t) \in \mathbb{R}^D$, with D equal to 2 or 3. As we see later, extending the state to include, for instance, the velocity, gives us more flexibility for imposing motion priors. At given times $t_n, n = 1, \dots, N$, we obtain distance measurements d_{mn} from the position $x_n := x(t_n)$ to known anchors $y_m \in \mathbb{R}^D, m = 1, \dots, M$. The number of observed anchors from position n is denoted by M_n , with $E = \sum_n M_n$ the total number of measurements. The measurement model is thus

$$\mathbf{h}_n(\theta_n) = \begin{bmatrix} \|y_1 - x_n\|^2 \\ \vdots \\ \|y_{M_n} - x_n\|^2 \end{bmatrix} = \begin{bmatrix} d_{1n}^2 \\ \vdots \\ d_{M_n n}^2 \end{bmatrix}, \quad (1)$$

with $\theta_n := \theta(t_n)$ and d_{mn} the distance from anchor m to position n . We denote the noisy measurements by $\tilde{d}_n := \mathbf{h}_n(\theta_n) + \mathbf{n}_n$, with \mathbf{n}_n measurement noise with covariance Σ_n . We introduce the matrix of known anchor coordinates $\mathbf{Y}_n = [y_1 \cdots y_{M_n}] \in \mathbb{R}^{D \times M_n}$ and the vector of its squared norms $\gamma_n^\top = [\|y_1\|^2 \cdots \|y_{M_n}\|^2] \in \mathbb{R}^{M_n}$. \mathbf{I}_d and $\mathbf{1}_d$ are the d -dimensional identity matrix and the vector of all ones, respectively, and \mathbf{i}_n^d is the length- d selection vector with a one at index n . Finally, we write all time-concatenated vectors as

$\mathbf{x}^\top = [\mathbf{x}_1^\top \cdots \mathbf{x}_N^\top]$, and the block-diagonal matrix composed of elements \mathbf{A}_n as $\text{Diag}(\mathbf{A}_n)_{n=1}^N$. The Kronecker product is written as \otimes , and $\mathbf{A} \succeq 0$ signifies \mathbf{A} is a positive-semidefinite (PSD) matrix.

B. Certified Multilateration

We first derive a certificate for range-only localization without imposing any smoothness on the trajectory. Therefore, we assume that our state is discrete and consists only of the position: $\boldsymbol{\theta}_n = \mathbf{x}_n \in \mathbb{R}^D$. The problem could be separated into N smaller problems, each of which has an optimal solution [9], [10], but treating it jointly serves as a convenient starting point for the continuous-time certificates.

a) *Problem Statement:* The MAP estimate can be obtained by solving

$$\hat{\boldsymbol{\theta}} = \min_{\boldsymbol{\theta}} f(\boldsymbol{\theta}) = \min_{\boldsymbol{\theta}} \frac{1}{E} \sum_n \mathbf{e}_n^\top \boldsymbol{\Sigma}_n^{-1} \mathbf{e}_n, \quad (2)$$

with $\mathbf{e}_n = \tilde{\mathbf{d}}_n - \mathbf{h}_n(\boldsymbol{\theta}_n)$.¹ Expanding row m of the error vector \mathbf{e}_n yields

$$\begin{aligned} e_{mn} &= \tilde{d}_{mn}^2 - \|\mathbf{y}_m - \mathbf{x}_n\|^2 \\ &= \tilde{d}_{mn}^2 - \|\mathbf{y}_m\|^2 + 2\mathbf{y}_m^\top \mathbf{x}_n - \|\mathbf{x}_n\|^2, \end{aligned} \quad (3)$$

which shows that (2) is a quartic function in the unknown vectors \mathbf{x}_n . To turn it into a quadratic function, we introduce the substitution $z_n = \|\mathbf{x}_n\|^2$. Then, using $\mathbf{f}_n^\top := [\mathbf{x}_n^\top \ z_n]$ and $\mathbf{b}_n := \tilde{\mathbf{d}}_n - \gamma_n$ we can rewrite the error vector as $\mathbf{e}_n = \mathbf{Q}_n \mathbf{f}_n + \mathbf{b}_n$, with $\mathbf{Q}_n := [2\mathbf{Y}_n^\top \ -1]$. We obtain the following quadratically-constrained quadratic program (QCQP), equivalent to (2):

$$\begin{aligned} \min_{\mathbf{f}_n, n=1,\dots,N} \quad & \frac{1}{E} \sum_n (\mathbf{Q}_n^\top \mathbf{f}_n + \mathbf{b}_n)^\top \boldsymbol{\Sigma}_n^{-1} (\mathbf{Q}_n^\top \mathbf{f}_n + \mathbf{b}_n) \\ \text{s.t. } \mathbf{f}_n^\top \begin{bmatrix} \mathbf{I}_d & \mathbf{0} \\ \mathbf{0}^\top & 0 \end{bmatrix} \mathbf{f}_n - [\mathbf{0}^\top \ 1] \mathbf{f}_n &= 0 \quad n = 1, \dots, N. \end{aligned} \quad (4)$$

Introducing $\mathbf{f} \in \mathbb{R}^F$, the vector of stacked variables of size $F = N(D+1) + 1$,

$$\mathbf{f}^\top = [\mathbf{x}_1^\top \ z_1 \ \cdots \ \mathbf{x}_N^\top \ z_N \ \ell], \quad (5)$$

with ℓ a homogenization variable, we can convert (4) into the standard, homogeneous QCQP:

$$\begin{aligned} (\text{Q}) \quad q^* &= \min_{\mathbf{f}} \frac{1}{E} \mathbf{f}^\top \mathbf{Q} \mathbf{f} \\ \text{s.t. } \mathbf{f}^\top \mathbf{A}_n \mathbf{f} &= 0 \quad n = 1, \dots, N \\ \mathbf{f}^\top \mathbf{A}_0 \mathbf{f} &= 1, \end{aligned} \quad (6)$$

with $\mathbf{A}_0 \in \mathbb{R}^{F \times F}$ the all-zero matrix except for a one for the bottom-right element, and $\mathbf{A}_n, \mathbf{Q} \in \mathbb{R}^{F \times F}$ given by

$$\mathbf{A}_n = \mathbf{S}_n \begin{bmatrix} \mathbf{I}_d & \mathbf{0} & \mathbf{0} \\ \mathbf{0}^\top & 0 & -\frac{1}{2} \\ \mathbf{0}^\top & -\frac{1}{2} & 0 \end{bmatrix} \mathbf{S}_n^\top, \quad \mathbf{S}_n = \begin{bmatrix} \mathbf{i}_n^N \otimes \mathbf{I}_{d+1} & \mathbf{0} \\ \mathbf{0}^\top & 1 \end{bmatrix}, \quad (7)$$

¹We use $\boldsymbol{\theta}$ instead of \mathbf{x} , although the state only contains the position, to make the extension to the next Section more apparent.

$$\begin{aligned} \mathbf{Q} &= \begin{bmatrix} \mathbf{Q}_{11} & \cdots & \mathbf{0} & \mathbf{q}_1 \\ \vdots & \ddots & \vdots & \vdots \\ \mathbf{0} & \cdots & \mathbf{Q}_{NN} & \mathbf{q}_N \\ \mathbf{q}_1^\top & \cdots & \mathbf{q}_N^\top & q_0 \end{bmatrix}, \quad q_0 = \sum_n \mathbf{b}_n^\top \boldsymbol{\Sigma}_n^{-1} \mathbf{b}_n, \\ \mathbf{Q}_{nn} &= \begin{bmatrix} 4\mathbf{Y}_n \boldsymbol{\Sigma}_n^{-1} \mathbf{Y}_n^\top & -2\mathbf{Y}_n \boldsymbol{\Sigma}_n^{-1} \mathbf{1} \\ -2\mathbf{1}^\top \boldsymbol{\Sigma}_n^{-1} \mathbf{Y}_n^\top & \mathbf{1}^\top \boldsymbol{\Sigma}_n^{-1} \mathbf{1} \end{bmatrix}, \quad \mathbf{q}_n = \begin{bmatrix} 2\mathbf{Y}_n \boldsymbol{\Sigma}_n^{-1} \mathbf{b}_n \\ -\mathbf{1}^\top \boldsymbol{\Sigma}_n^{-1} \mathbf{b}_n \end{bmatrix}. \end{aligned}$$

QCQP problems are non-convex and may be hard to solve optimally [24]. However, it is well known that we can exploit semidefinite relaxations, followed by Lagrangian duality theory, to analyze (or potentially compute globally optimal) solutions (see, e.g., [30], [29], [37]). Using this paradigm, we turn problem (Q) into a SDP by introducing $\mathbf{F} = \mathbf{f} \mathbf{f}^\top$ (which is equivalent to $\mathbf{F} \succeq 0$, $\text{rank } \mathbf{F} = 1$) and relaxing the rank constraint. This gives the standard SDP relaxation of (Q), which we denote as the primal problem (P) [24]:

$$\begin{aligned} (\text{P}) \quad p^* &= \min_{\mathbf{F}} \frac{1}{E} \text{tr}(\mathbf{Q}^\top \mathbf{F}) \\ \text{s.t. } \text{tr}(\mathbf{A}_n \mathbf{F}) &= 0 \quad n = 1, \dots, N \\ \text{tr}(\mathbf{A}_0 \mathbf{F}) &= 1 \\ \mathbf{F} &\succeq 0. \end{aligned} \quad (8)$$

The (Lagrangian) dual problem [24] is given by

$$\begin{aligned} (\text{D}) \quad d^* &= \max_{\rho, \boldsymbol{\lambda}} (-\rho) \\ \text{s.t. } \mathbf{H}(\rho, \boldsymbol{\lambda}) &:= \frac{1}{E} \mathbf{Q} + \sum_n \lambda_n \mathbf{A}_n + \rho \mathbf{A}_0 \succeq 0, \end{aligned} \quad (9)$$

where ρ and $\boldsymbol{\lambda}^\top = [\lambda_1 \cdots \lambda_N] \in \mathbb{R}^N$ are called the Lagrange multipliers or dual variables.

At this point, it is useful to take a step back and consider what we have achieved so far. We have relaxed our original nonlinear state estimation into a standard SDP. Now, we could take at least two different approaches to solving the original problem:

- Solve the relaxed problem (P), and investigate the solution, denoted by \mathbf{F}^* . If the obtained solution has rank 1, then we can decompose it into $\mathbf{F}^* = \mathbf{f}^* \mathbf{f}^{*\top}$, where \mathbf{f}^* is exactly the globally optimal solution to (Q).
- Solve the primal problem (Q) locally using an iterative nonlinear solver. This will return a solution that is ensured to be locally optimal; we call this estimate $\hat{\mathbf{f}}$. Then, we can use optimality conditions from duality theory to derive a certificate for this solution: if the certificate holds, the solution is in fact optimal and we have $\hat{\mathbf{f}} = \mathbf{f}^*$.

In this paper, we take the second approach. This choice is motivated by two observations. First, in standard localization problems, we aim to solve for a large number of points simultaneously, yielding a large SDP for (P). The typical complexity of available solvers is cubic in the number of points [6], making them too slow for real-time robotics applications. Second, we found that even a basic iterative solver often converges to the optimal solution, in particular for the noise levels that are adequate for localization problems. As we will show, such solvers can exploit the sparsity of the problem in a principled manner, which makes them significantly faster than

SDP solvers. A similar approach was used in recent works to certify the solutions of other common problems in robotics such as pose-graph optimization [29] and landmark-based SLAM [29], [38]. These problems assume linear measurement models, while we treat non-linear distance measurements.

b) Certificate: Our aim is to determine whether a locally optimal solution $\hat{\mathbf{f}}$ to (Q) is also the global optimum. We obtain a local solution $\hat{\mathbf{x}}$ to (2) from a standard iterative GN solver, as outlined in III-D, and augment it to $\hat{\mathbf{f}}$ as in (5). We know from duality theory (see *e.g.*, [37]) that if we can find dual variables $\hat{\rho}, \hat{\lambda}$ such that:

$$\hat{\mathbf{f}}^\top \mathbf{A}_0 \hat{\mathbf{f}} = 1, (\forall n) \hat{\mathbf{f}}^\top \mathbf{A}_n \hat{\mathbf{f}} = 0 \text{ (primal feasibility),} \quad (10)$$

$$\mathbf{H}(\hat{\rho}, \hat{\lambda}) \succeq 0 \text{ (dual feasibility), and} \quad (11)$$

$$\mathbf{H}(\hat{\rho}, \hat{\lambda}) \hat{\mathbf{f}} = \mathbf{0} \text{ (stationarity condition),} \quad (12)$$

then $\hat{\mathbf{f}}$ (and thus $\hat{\mathbf{x}}$) is in fact the optimal solution to (Q). Because $\mathbf{H}(\hat{\rho}, \hat{\lambda})$ plays such a crucial role, we will refer to it as the ‘certificate matrix’. Note that the conditions are sufficient, but not necessary – if a solution does not satisfy all conditions it may still be an optimal solution. However, related works have shown that for sufficiently low noise levels, strong duality holds, and the certificate becomes both sufficient *and* necessary [37]. This is confirmed and further discussed in the simulated experiments in Section IV-A.

The primal feasibility is trivial by construction, so we only need to verify the last two conditions. We can rewrite the stationarity condition as

$$[\mathbf{A}_1 \hat{\mathbf{f}} \quad \cdots \quad \mathbf{A}_N \hat{\mathbf{f}} \quad \mathbf{A}_0 \hat{\mathbf{f}}] \hat{\mathbf{y}} = -\frac{1}{E} \mathbf{Q} \hat{\mathbf{f}}, \quad (13)$$

with $\hat{\mathbf{y}} := [\hat{\lambda}_1 \quad \cdots \quad \hat{\lambda}_N \quad \hat{\rho}]^\top$, which is a linear system with F equations and $N + 1$ unknowns, and a priori, may not have a solution. However, we show in the supplementary material [39] that the system admits the unique solution:

$$(\forall n) \quad \hat{\lambda}_n = -2 \frac{1}{E} \mathbf{1}^\top \Sigma_n^{-1} \mathbf{e}_n, \quad (14)$$

$$\hat{\rho} = -\frac{1}{E} \sum_n \mathbf{e}_n^\top \Sigma_n^{-1} \mathbf{e}_n. \quad (15)$$

Note that the analytical solution of $\hat{\rho}$ shows that strong duality holds between (Q) and (D) provided (11) is true, as we have $d^* = -\hat{\rho} = q^*$.

In summary, given a locally optimal solution $\hat{\mathbf{f}}$, we can use (14) and (15) to solve for the optimal dual variables. If they are such that the certificate matrix is PSD, all conditions (10) to (12) are satisfied and we conclude that $\hat{\mathbf{f}}$ is in fact the optimal solution to (P).

C. Certified Continuous-Time Range-Only Localization

The previous example has taught us how to certify the optimality of a candidate solution to the range-only localization problem. However, we reiterate that efficient optimal solvers for problem (2) exist, therefore locally solving and then certifying the solution is not necessary in general.

However, we can use what we have learned to extend the method to incorporate motion priors, a case for which no efficient, provably optimal solvers are known. Instead of an

optimal solver, the certificates developed hereafter allow us to use a local solver, followed by a certificate check, both of which can be implemented efficiently by exploiting sparsity. As we will see in Section IV, the fast local solver finds the global optimum most of the time, and suboptimal solutions can be avoided through simple reinitialization; our certificate can tell us when this is necessary.

a) Motion Prior: Since robots move according to physical laws, the resulting trajectories typically exhibit a certain degree of smoothness. A principled way to formalize this fact is by expressing the trajectory as a GP, with a one-to-one correspondence between both the covariance and mean functions and the motion prior. Following the method outlined in [12], we show in this Section that we can incorporate a motion prior in our MAP estimation by solving:

$$\hat{\boldsymbol{\theta}} = \min_{\boldsymbol{\theta}} f(\boldsymbol{\theta}) + r(\boldsymbol{\theta}), \quad (16)$$

where $f(\boldsymbol{\theta})$ is defined in (2), and $r(\boldsymbol{\theta})$ is a regularization term enforcing the prior. In the following sections, we will show that we can use a similar methodology as in multilateration to certify solutions to problem (16).

In contrast with Section III-B, the state vector $\boldsymbol{\theta}(t) \in \mathbb{R}^K$ may now consist of more states than just the position; for instance, we may add velocity and even acceleration. We assume that $\boldsymbol{\theta}(t)$ is a GP:

$$\boldsymbol{\theta}(t) \sim \mathcal{GP}(\boldsymbol{\mu}(t), \mathbf{K}(t, t')), \quad t_0 < t, t' \quad (17)$$

where $\boldsymbol{\mu}(t)$ is the mean function, $\mathbf{K}(t, t')$ is the covariance function between two times, and t_0 is the starting time. We set the prior mean function to zero, as is commonly done in practice. One particular class of covariance functions comes from assuming a linear, time-varying (LTV) system:

$$\dot{\boldsymbol{\theta}}(t) = \mathbf{A}(t)\boldsymbol{\theta}(t) + \mathbf{B}(t)\mathbf{u}(t) + \mathbf{F}(t)\mathbf{w}(t), \quad (18)$$

with $\mathbf{A}(t)$, $\mathbf{B}(t)$ and $\mathbf{F}(t)$ known system matrices, $\mathbf{u}(t)$ a known input and $\mathbf{w}(t) \sim \mathcal{GP}(\mathbf{0}, \mathbf{Q}_C \delta(t - t'))$, a stationary zero-mean GP with power spectral density matrix \mathbf{Q}_C . The general solution to this model is

$$\boldsymbol{\theta}(t) = \Phi(t, t_0)\boldsymbol{\theta}(t_0) + \int_{t_0}^t \Phi(t, s)(\mathbf{B}(s)\mathbf{u}(s) + \mathbf{F}(s)\mathbf{w}(s))ds, \quad (19)$$

where $\Phi(t, t')$ is the transition function. To make the model more tangible, we introduce two example motion priors.

Example 1: zero-velocity prior By setting the state to the position only ($\boldsymbol{\theta}(t) = \mathbf{x}(t)$), and the system matrices to $\mathbf{A}(t) = \mathbf{F}(t) = \mathbf{I}$, and $\mathbf{B}(t) = \mathbf{0}$, we obtain the ‘zero-velocity’ prior, meaning we assume that there is no motion between two consecutive points. In this case, the transition matrix is simply $\Phi(t, t') = \mathbf{I}$, and we obtain a regularization term equivalent to Tikhonov regularization [40].

Example 2: constant-velocity prior The constant-velocity assumption is imposed by setting:

$$\boldsymbol{\theta}(t) = \begin{bmatrix} \mathbf{x}(t) \\ \mathbf{v}(t) \end{bmatrix}, \mathbf{A}(t) = \begin{bmatrix} \mathbf{0} & \mathbf{I} \\ \mathbf{0} & \mathbf{0} \end{bmatrix}, \mathbf{B}(t) = \mathbf{0}, \mathbf{F}(t) = \begin{bmatrix} \mathbf{0} \\ \mathbf{I} \end{bmatrix},$$

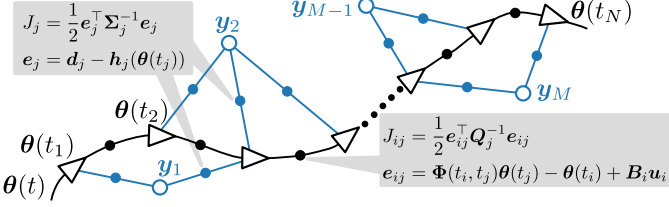


Fig. 2: Factor graph representation of the GP inference problem. Black factors represent the motion prior, blue are the range-only measurement factors.

where $v(t)$ denotes the velocity at time t . In this case, the transition matrix is

$$\Phi(t, t') = \begin{bmatrix} \mathbf{I} & (t - t')\mathbf{I} \\ \mathbf{0} & \mathbf{I} \end{bmatrix}. \quad (20)$$

Any higher-order priors from the LTV family, such as white-noise-on-jerk (constant-acceleration) priors, can be derived analogously [12]. For all of these priors, the regularization term takes the form

$$r(\theta) := \frac{1}{N} \sum_{n=2}^N e_{n,n-1} Q_n^{-1} e_{n,n-1}, \quad (21)$$

where we have introduced

$$e_{n,n-1} := \Phi_{n,n-1} \theta_{n-1} - \theta_n + B_n u_n \quad (22)$$

$$u_n := \int_{t_{n-1}}^{t_n} \Phi(t_n, s) B(s) u(s) ds \quad (23)$$

$$Q_n := \int_{t_{n-1}}^{t_n} \Phi(t_n, s) F(s) Q_c F(s)^\top \Phi(t_n, s)^\top ds, \quad (24)$$

and $\theta_n := \theta(t_n)$, $B_n := B(t_n)$, and $\Phi_{ij} := \Phi(t_i, t_j)$. The important point to note is that each regularization term in (16) depends only on two adjacent states, owing to the Markov property. The inference problem is thus still sparse, which we will exploit later to develop efficient solvers. To visualize this point, we show in Figure 2 the factor-graph representation of the inference problem. The GP prior results in state-to-state factors, taking a similar role as odometry measurements would in classical SLAM problems.

b) *Problem Statement:* We have now derived all ingredients to bring the estimation problem with motion prior into a standard QCQP. First, we note that $r(\theta)$ can be written as

$$r(\theta) = \frac{1}{N} \theta^\top R \theta, \quad (25)$$

where R is the block-tridiagonal matrix with off-diagonal elements $R_{n,n+1} = -\Phi_{n+1,n}^\top Q_{n+1}^{-1} \Phi_{n+1,n}$ for $1 \leq n \leq N-1$ and diagonal elements

$$R_{nn} = \begin{cases} Q_n^{-1} + \Phi_{n+1,n}^\top Q_{n+1}^{-1} \Phi_{n+1,n} & \text{for } 2 \leq n \leq N-1 \\ \Phi_{n+1,n}^\top Q_{n+1}^{-1} \Phi_{n+1,n} & \text{for } n = 1 \\ Q_n^{-1} & \text{for } n = N \end{cases}. \quad (26)$$

We also introduce the new vector $\mathbf{g}^\top = [\theta_1^\top \ z_1 \ \dots \ \theta_N^\top \ z_N \ 1]$ where we do not add any substitution variables for the components of θ_n other than x_n because the added regularization is already quadratic in θ_n . We then augment R with zero rows and columns

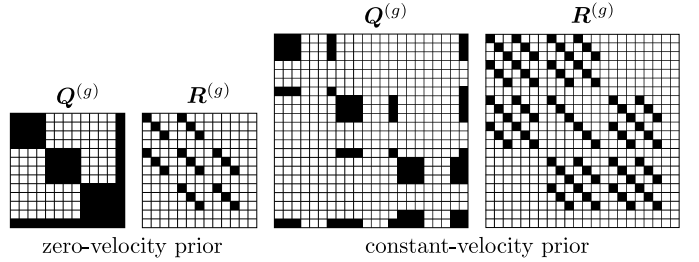


Fig. 3: Sparsity patterns of the cost matrices obtained using zero-velocity or constant-velocity priors, for $N = 3$ and $D = 3$.

where the regularization is zero (i.e., for the substitution variables), yielding $R^{(g)}$. Similarly, we create $Q^{(g)}$ and $A_i^{(g)}$, $i = 0, \dots, N$ by padding with zeros for the variables in θ_n other than the position. Finally, we can write (16) in the standard form

$$\begin{aligned} (\text{Q-GP}) \quad q_{GP}^* = \min_{\mathbf{g}} \frac{1}{E} \mathbf{g}^\top Q^{(g)} \mathbf{g} + \frac{1}{N} \mathbf{g}^\top R^{(g)} \mathbf{g} \\ \text{s.t. } \mathbf{g}^\top A_n^{(g)} \mathbf{g} = 0 \quad n = 1, \dots, N \\ \mathbf{g}^\top A_0^{(g)} \mathbf{g} = 1. \end{aligned} \quad (27)$$

We show examples of the zero-padded cost matrices, using the two example motion priors, in Figure 3.

c) *Certificate:* Comparing (Q-GP) with (Q) it is clear that a new certificate can be derived by checking conditions (10) to (12), but with the new system matrices. In particular, we define the new certificate matrix

$$H_{GP}(\hat{\rho}, \hat{\lambda}) = \frac{1}{E} Q^{(g)} + \frac{1}{N} R^{(g)} + \hat{\rho} A_0^{(g)} + \sum_n \hat{\lambda}_n A_n^{(g)}. \quad (28)$$

We note again that primal feasibility (10) is given by construction. The stationarity condition (12) now reads

$$\begin{bmatrix} A_1^{(g)} \hat{\mathbf{g}} & \dots & A_N^{(g)} \hat{\mathbf{g}} & A_0^{(g)} \hat{\mathbf{g}} \end{bmatrix} \hat{\mathbf{y}} = -\frac{1}{E} Q^{(g)} \hat{\mathbf{g}} - \frac{1}{N} R^{(g)} \hat{\mathbf{g}}. \quad (29)$$

As in Section III-B, we show in the supplementary material [39] that this system of equations has a unique solution, given by (14) for $\hat{\lambda}$ and

$$\hat{\rho} = -\frac{1}{E} \sum_n e_n^\top \Sigma_n^{-1} e_n - \frac{1}{N} \hat{\theta}^\top R \hat{\theta}. \quad (30)$$

Again, if the dual variables are feasible, then (30) implies strong duality.

D. Iterative Solver

The proposed certificate is applicable to any solution candidate satisfying first-order stationarity. A number of nonlinear least-squares solvers could be used to obtain such a candidate [6]. We give a brief outline of our implemented sparse GN solver, which we choose because of its wide usage and efficiency. Linearizing the least-squares residuals around a current estimate θ^k , the optimal update $\delta\theta$ is the solution of

$$\left(R + \frac{N}{E} J^\top \Sigma^{-1} J \right) \delta\theta = -R\theta^k + \frac{N}{E} J^\top \Sigma^{-1} (d - h(\theta^k)). \quad (31)$$

Here, $J := \text{Diag}(\nabla_{x_n} h_n)_{n=1}^N$ is the measurement Jacobian, and $\Sigma^{-1} := \text{Diag}(\Sigma_n^{-1})_{n=1}^N$. The vector d contains all

stacked distance measurements $\mathbf{d}^\top = [d_1^\top \cdots d_N^\top]$. We refer the reader to [11, 4.4.3] for a detailed treatment of GN for continuous-time estimation. We stop the algorithm when the root-mean-squared step size is less than 10^{-10} . Equation (31) is a sparse linear system of equations due to the form of the left-hand-side matrices, and can be solved efficiently via, for instance, sparse Cholesky factorization. The complexity of each iteration is thus $O(N)$ and we found that in practice, convergence usually takes less than 10 iterations.

E. Efficient Certificate Computation

For a practical solution, we require not only an efficient iterative solver, but also an efficient certificate. Since we can solve analytically for the optimal dual variables in $O(N)$ time, the bottleneck of the computation lies in certifying PSD-ness of the certificate matrix, which is of size $N(K + 1) + 1$. The most intuitive approach of computing the eigenvalues of this matrix is prohibitively expensive, with complexity of up to $O(N^3)$ [41]. Thankfully, we can exploit the particular sparsity pattern of the matrix to bring the cost of the certificate down to $O(N)$, as we will outline next.

The certificate matrix is a block-tridiagonal arrowhead matrix and belongs to the class of chordally sparse matrices, which exhibit numerous interesting properties (see [42] for an overview). The chordal property we exploit here is that the sparsity pattern is ‘preserved’ in the \mathbf{L} matrix of the \mathbf{LDL}^\top decomposition. For our sparsity pattern, the certificate matrix is PSD, if and only if it can be decomposed as $\mathbf{H} = \mathbf{LDL}^\top$, with $\mathbf{D} = \text{Diag}([(D_n)_{n=1}^N, \delta])$, and

$$\mathbf{L} = \begin{bmatrix} \mathbf{J}_1 & \mathbf{0} & \cdots & \cdots & \mathbf{0} \\ \mathbf{L}_1 & \ddots & \ddots & & \vdots \\ \vdots & \ddots & \ddots & \ddots & \vdots \\ \mathbf{0} & \cdots & \mathbf{L}_{N-1} & \mathbf{J}_N & \mathbf{0} \\ \mathbf{l}_1^\top & \cdots & \mathbf{l}_{N-1}^\top & \mathbf{l}_N^\top & 1 \end{bmatrix}, \quad (32)$$

where \mathbf{J}_n are lower-diagonal matrices and \mathbf{D}_n are diagonal matrices with non-negative elements. \mathbf{L}_n and \mathbf{l}_n are a priori dense matrices and vectors, respectively. Equating the non-zero elements in (32) with the corresponding blocks of $\mathbf{H}(\hat{\rho}, \hat{\lambda})$, we obtain the following equalities:

$$\begin{aligned} \mathbf{H}_{nn} &= \begin{cases} \mathbf{J}_n \mathbf{D}_n \mathbf{J}_n^\top & \text{for } n = 1 \\ \mathbf{L}_{n-1} \mathbf{D}_{n-1} \mathbf{L}_{n-1}^\top + \mathbf{J}_n \mathbf{D}_n \mathbf{J}_n^\top & \text{for } 2 \leq n \leq N \end{cases}, \\ \mathbf{h}_n &= \begin{cases} \mathbf{J}_n \mathbf{D}_n \mathbf{l}_n & \text{for } n = 1 \\ \mathbf{L}_{n-1} \mathbf{D}_{n-1} \mathbf{l}_{n-1} + \mathbf{J}_n \mathbf{D}_n \mathbf{l}_n & \text{for } 2 \leq n \leq N \end{cases}, \\ \mathbf{H}_{n,n+1} &= \mathbf{J}_n \mathbf{D}_n \mathbf{L}_n^\top \quad \text{for } 1 \leq n \leq N-1, \\ \mathbf{h} &= \sum_{n=1}^N \mathbf{l}_n^\top \mathbf{D}_n \mathbf{l}_n + \delta. \end{aligned} \quad (33)$$

These equations define a recursive scheme for computing the decomposition; the unknown factors can be computed in the order $\mathbf{D}_1, \mathbf{J}_1, \mathbf{L}_1, \dots, \mathbf{D}_N, \mathbf{J}_N, \mathbf{L}_N, \mathbf{l}_1, \dots, \mathbf{l}_N, \delta$. The factors \mathbf{D}_n and \mathbf{J}_n are computed through individual \mathbf{LDL}^\top decompositions, but the involved matrices are only of size $K + 1$. We can stop computing the decomposition early if we find a negative diagonal value, as the certificate has failed. The

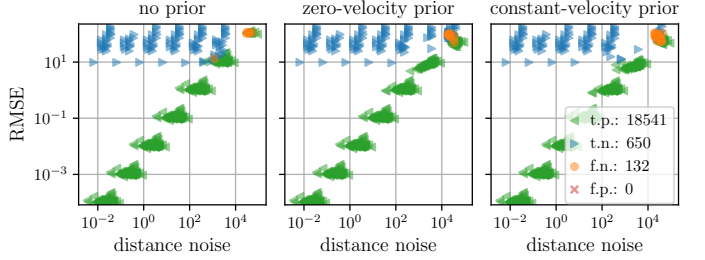


Fig. 4: Certificate value vs. root-mean-squared error (RMSE), using different motion priors, in simulations with $N = 100$, $M = 6$ and $D = 2$. The group of solutions corresponding to the smallest cost out of 10 initializations are labelled optimal. Disregarding the highest noise levels, all optimal solutions are successfully identified (true positives, t.p.) and the certificate fails for suboptimal solutions (true negatives, t.n.). At the highest noise levels, a small proportion of optimal solutions are not certified (false negatives, f.n.), which is in line with the sufficiency of the certificate.

algorithm runs in $O(N)$ and as we show in simulation, has a similar absolute runtime as the GN solver².

IV. EXPERIMENTAL RESULTS

In this section, we show the effectiveness of the proposed method in simulation and on a real-world dataset. We first study the certificate in simulation, showing that our local solver finds the optimal solution in the majority of cases for random setups, and when it fails to do so, the certificate does not hold for all but the highest considered noise levels. Incorrect local solutions are typically only found for few random initializations, suggesting that in practice, randomly reinitializing until the certificate holds is a viable strategy. Next, we use the certificate to evaluate the localization performance in a real-world scenario with distance measurements from UWB anchors measured on a drone and show that we can successfully differentiate local and global solutions³.

A. Simulation Results

a) *Setup*: We create 2D simulated experiments by generating trajectories according to the constant-velocity model, where for each random instance we draw an initial velocity and position vector uniformly and coordinate-wise from $[-1, 1]$. Note that we consider all dimensions normalized thus unitless. The noise on the acceleration is assumed independent with $\sigma_a = 0.2$, so that $\mathbf{Q}_C = \sigma_a \mathbf{I}$. The anchor coordinates are also drawn uniformly at random from $[0, 1]$ and their bounding box is scaled to the size of the trajectory. We set $N = 100$ and $M = 6$. We measure distances from all anchors at each time, and we generate measurements by adding Gaussian noise to

²In practice, the decomposition may suffer from numerical instability [41, Section 4.2], meaning that when the smallest eigenvalue of \mathbf{H} is slightly negative, the diagonal elements of \mathbf{D} may become strongly negative, wrongly indicating a failed certificate. To mitigate this fact, we add a small regularization $\mathbf{H} \leftarrow \mathbf{H} + \beta \mathbf{I}$ before computing the decomposition. We set the value to $\beta = 1e-3$ throughout the real-world experiments. However, preliminary experiments suggest that different anchor configurations may require a different threshold. Automatic tuning of β or a more numerically stable certification method are subjects of current investigation.

³The Python code to reproduce all results is available at https://github.com/utiasASRL/safe_and_smooth.

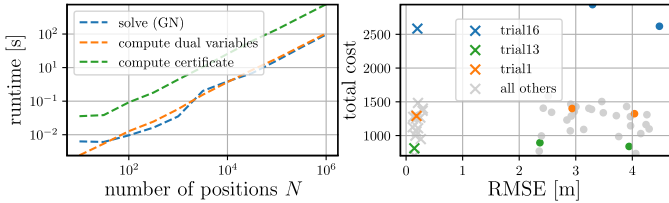


Fig. 5: Left: Computation time of our GN solver, evaluating the dual variables, and computing the certificate, respectively, with increasing number of positions N . Right: certificate evaluation on real data, comparing the final cost and RMSE of solutions. Three solutions for three chosen datasets are highlighted in colors. For all datasets, the cost difference between certified solutions (cross) and uncertified solutions (circle) is small, but the resulting RMSE difference is significant. Thanks to the proposed method, such suboptimal solutions can be avoided.

the true distances before squaring them. We assume *i.i.d.* zero-mean noise with variance σ_d . For each random experimental setup, we solve using the GN algorithm, using 10 different random initializations, and using no motion prior, a zero-velocity motion prior and a constant-velocity motion prior, respectively. We set Σ_n and Q_C to the true values.

b) *Results:* First, we study the effect of noise in a quantitative analysis in Figure 4. We vary the measurement noise σ_d and report the RMSE between the estimated and ground-truth trajectory as a function of the effective distance noise. Since we lack an optimal solver, we label solutions as globally optimal when they correspond to the smallest cost (up to numerical tolerance) for a given setup, and locally optimal otherwise. This method is reliable for small noise levels, as a big gap exists between the cost of the local and global solutions, but less so for higher noise. Using this method, we can identify that the majority of solutions (96%) are true positives — global solutions where the certificate holds. Even more importantly, we observe that there are no false positives — the certificate never holds for a suboptimal solution. Out of the uncertified solutions, 20% are false negatives, meaning the certificate misses an optimal solution. However, this happens only at the highest noise levels considered, suggesting the existence of a high noise threshold up to which strong duality holds. For lower noise levels, we conclude that although the certificate is only a sufficient condition in theory, it is effectively a necessary condition in practice: when the certificate does not hold, the solution is usually suboptimal. We also note that the method and certificate are robust to model mismatch: although the real trajectory is of the constant-velocity type, all motion priors yield satisfactory results. A study of the setups leading to local optima, given in the supplementary material [39], reveals that local minima are usually the result of poor (*i.e.*, almost co-linear) anchor placement.

We also study the computation time with increasing number of positions N . The left plot of Figure 5 shows that both the computation times of the solver and certificate increase linearly with N . While the certificate takes slightly longer than GN on average, this difference may be reduced by a more efficient implementation. We run our method on up to a million states (using the highest-dimensional constant-velocity prior), underlining the scalability of the approach.

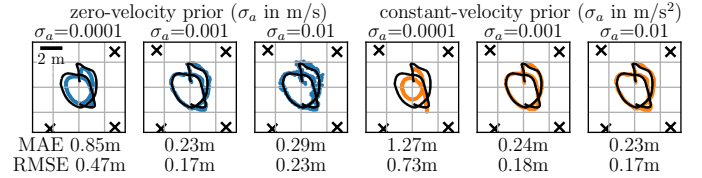


Fig. 6: Planar projections of certified solutions for the first flying drone dataset, using the zero-velocity prior (blue) and the constant-velocity prior (orange), with varying parameter σ_a . The ground truth is shown in black, and the RMSE and mean absolute error (MAE) are shown below each plot. The motion prior has to strike a balance between over-smoothing and over-fitting to noisy measurements. We find that the constant-velocity prior with $\sigma_a = 1e^{-3}$ m/s² yields consistent results for all datasets.

B. Experimental UWB Drone Dataset

Finally, we test the certificate on a dataset collected by a drone in a flying arena. We use $M = 4$ UWB anchors, placed in the 4 top corners of an arena, which is about 7 by 7 meters wide and 3 meters high. Measurements are obtained asynchronously, resulting in exactly one distance measurement at a time. Ground truth position is obtained with a *Vicon* motion capture setup. The setup is described in more detail in [43]. In total, 16 different flights (trials), are performed, with different trajectory characteristics and varying velocities, using a constant-acceleration policy. The average measurement frequency per anchor is 5 Hz, and each trial being a bit more than one minute long, we obtain about $N = 1600$ measurement times for each trial. The average runtime of our estimation algorithm including certificate is 5 s, of which 3.5 s are spent on certification. The bias in the distance measurements, typical for UWB measurements, is removed in a prior calibration phase.

Since the motion model is unknown a priori, we perform calibration on the first dataset to identify suitable values for σ_a (we fix σ_d to 5 cm according to the expected accuracy of the UWB anchors). Figure 6 shows the estimates obtained using different combinations of σ_a and motion priors; We use the constant-velocity prior and $\sigma_a = 1e^{-3}$ m/s², for a good balance between smoothing and overfitting to noise, which is reflected in a low RMSE and MAE, respectively.

Figure 1 shows two example estimates for the first dataset, both of which correspond to stationary points of the problem, with one corresponding to the global minimum and one to a local minimum with high RMSE. The certificate successfully identifies the global minimum, and it does not hold for the local minimum. The same behavior is observed on all datasets, which are summarized in Figure 5. Note that all certified solutions, marked with crosses, correspond to a significantly lower RMSE than the local solutions, for which the certificate does not hold. The cost, on the other hand, is quite similar between global and local minima (three examples are highlighted in Figure 5), which suggests that it cannot be used for automatically evaluating optimality. Like in the simulated measurements, we observe that the local solution seems to be the result of poor anchor placement: the anchors are almost co-planar. Indeed, when using measurements from two additional ground-based anchors, it was found that the local solution always converges to the global optimum.

V. CONCLUSION AND FUTURE WORK

We have provided optimality certificates for range-only continuous-time localization. We have derived a closed-form solution for the optimal Lagrange multipliers that depends only on the residuals of the problem, and provided an efficient method for checking if the certificate matrix is PSD. We have successfully certified the solutions found by a sparsity-exploiting GN solver both in simulation and real experiments, and observed that the global optimum is found in most cases, in particular when the anchors are placed in non-degenerate configurations. We hope that the proposed certificate is a first step to extend existing provably optimal solvers to distance and other nonlinear measurements. A promising line of future work is the extension of the results to the full SLAM setup, where the anchor positions are unknown a priori. In a second step, the sparsity of the problem suggests that incorporating certificates into incremental solvers such as [18] could decrease the computational cost of the proposed method even further. Finally, the least-squares formulation used herein is sensitive to outliers, and could be replaced with a more robust cost function [34], [32].

ACKNOWLEDGMENTS

We would like to thank Abhishek Goudar of the Dynamic Systems Lab for providing us with the drone dataset.

REFERENCES

- [1] A. Raza, L. Lolic, S. Akhter, and M. Liut, “Comparing and evaluating indoor positioning techniques,” in *IPIN*, 2021.
- [2] J. Djugash, B. Hamner, and S. Roth, “Navigating with ranging radios: Five data sets with ground truth,” *Journal of Field Robotics*, vol. 26, no. 9, pp. 689–695, 2009.
- [3] W. Shule, C. M. Almansa, J. P. Queraltà, Z. Zou, and T. Westerlund, “UWB-based localization for multi-UAV systems and collaborative heterogeneous multi-robot systems,” *Procedia Computer Science*, vol. 175, pp. 357–364, 2020.
- [4] E. Olson, J. J. Leonard, and S. Teller, “Robust range-only beacon localization,” *IEEE J. Ocean. Eng.*, vol. 31, no. 4, pp. 949–2006, 2006.
- [5] M. Hamer and R. D’Andrea, “Self-calibrating ultra-wideband network supporting multi-robot localization,” *IEEE Access*, vol. 6, pp. 22 292–22 304, 2018.
- [6] J. Nocedal and S. J. Wright, *Numerical Optimization*, 2nd ed., ser. Springer Series in Operations Research. Springer-Verlag, 2006.
- [7] L. Liberti, C. Lavor, N. Maculan, and A. Mucherino, “Euclidean distance geometry and applications,” *SIAM Review*, vol. 56, no. 1, pp. 3–69, 2014.
- [8] A. M.-C. So and Y. Ye, “Theory of semidefinite programming for sensor network localization,” *Mathematical Programming*, vol. 109, no. 2-3, pp. 367–384, 2007.
- [9] M. Larsson, V. Larsson, K. Astrom, and M. Oskarsson, “Optimal trilateration is an eigenvalue problem,” in *IEEE ICASSP*, 2019, pp. 5586–5590.
- [10] A. Beck, P. Stoica, and J. Li, “Exact and approximate solutions of source localization problems,” *IEEE Trans. Signal Process.*, vol. 56, no. 5, pp. 1770–1778, 2008.
- [11] T. D. Barfoot, *State Estimation for Robotics*. Cambridge University Press, 2017.
- [12] T. Barfoot, C. Hay Tong, and S. Sarkka, “Batch continuous-time trajectory estimation as exactly sparse Gaussian process regression,” in *Robotics: Science and Systems*, 2014.
- [13] F. R. Fabresse, F. Caballero, I. Maza, and A. Ollero, “Undelayed 3D ROSLAM based on Gaussian-mixture and reduced spherical parametrization,” in *IEEE/RSJ IROS*, 2013, pp. 1555–1561.
- [14] G. Vallicrosa and P. Rida, “Sum of Gaussian single beacon range-only localization for AUV homing,” *Annual Reviews in Control*, vol. 42, pp. 117–187, 2016.
- [15] J.-L. Blanco, J.-A. Fernandez-Madrigal, and J. Gonzalez, “Efficient probabilistic range-only SLAM,” in *IEEE/RSJ IROS*, 2008, pp. 1017–1022.
- [16] J.-L. Blanco, J. Gonzalez, and J.-A. Fernandez-Madrigal, “A pure probabilistic approach to range-only SLAM,” in *IEEE ICRA*, 2008, pp. 1436–1441.
- [17] F. Dellaert and M. Kaess, “Square root SAM: Simultaneous localization and mapping via square root information smoothing,” *IJRR*, vol. 25, no. 12, pp. 1181–1203, 2006.
- [18] M. Kaess, H. Johannsson, R. Roberts, V. Ila, J. J. Leonard, and F. Dellaert, “iSAM2: Incremental smoothing and mapping using the bayes tree,” *IJRR*, vol. 31, no. 2, pp. 216–235, 2012.
- [19] M. Pacholska, F. Dümbgen, and A. Scholefield, “Relax and recover : Guaranteed range-only continuous localization,” *IEEE RAL*, vol. 5, no. 2, pp. 2248–2255, 2020.
- [20] P. Furgale, T. D. Barfoot, and G. Sibley, “Continuous-time batch estimation using temporal basis functions,” in *IEEE ICRA*, 2012, pp. 2088–2095.
- [21] P. Biswas and Y. Ye, “Semidefinite programming for ad hoc wireless sensor network localization,” in *International Symposium on Information Processing in Sensor Networks*, 2004, pp. 46–54.
- [22] P. Biswas, T.-C. Lian, T.-C. Wang, and Y. Ye, “Semidefinite programming based algorithms for sensor network localization,” *ACM Transactions on Sensor Networks*, vol. 2, no. 2, pp. 188–220, 2006.
- [23] I. Dokmanić, R. Parhizkar, J. Ranieri, and M. Vetterli, “Euclidean Distance Matrices: Essential theory, algorithms, and applications,” *IEEE Signal Processing Magazine*, vol. 32, no. 6, pp. 12–30, 2015.
- [24] S. Boyd and L. Vandenberghe, *Convex Optimization*. Cambridge University Press, 2004.
- [25] L. Carbone, D. Rosen, G. Calafiori, J. Leonard, and F. Dellaert, “Lagrangian duality in 3D SLAM: Verification techniques and optimal solutions,” in *IEEE/RSJ IROS*, 2015, pp. 125–132.
- [26] L. Carbone and F. Dellaert, “Duality-based verification techniques for 2D SLAM,” in *IEEE ICRA*, 2015, pp. 4589–4596.
- [27] J. Fredriksson and C. Olsson, “Simultaneous multiple rotation averaging using Lagrangian duality,” in *ACCV*, 2013, pp. 245–258.
- [28] J. Briales and J. Gonzalez-Jimenez, “Fast global optimality verification in 3D SLAM,” in *IEEE/RSJ IROS*, 2016, pp. 4630–4636.
- [29] D. M. Rosen, L. Carbone, A. S. Bandeira, and J. J. Leonard, “SE-sync: A certifiably correct algorithm for synchronization over the special euclidean group,” *IJRR*, vol. 38, no. 2-3, pp. 95–125, 2019.
- [30] A. Eriksson, C. Olsson, F. Kahl, and T.-J. Chin, “Rotation averaging and strong duality,” in *IEEE/CVF CVPR*, 2018, pp. 127–135.
- [31] F. Dellaert, D. M. Rosen, J. Wu, R. Mahony, and L. Carbone, “Shonan rotation averaging: Global optimality by surfing $SO(p)^n$,” in *European Conference on Computer Vision*, 2020, pp. 292–308.
- [32] T. D. Barfoot, C. Holmes, and F. Dümbgen, “A fine line: Total least-squares line fitting as QCQP optimization,” *arXiv:2206.05082*, Jun. 2022.
- [33] H. Yang, P. Antonante, V. Tzoumas, and L. Carbone, “Graduated non-convexity for robust spatial perception,” *IEEE RAL*, vol. 5, no. 2, pp. 1127–1134, 2020.
- [34] H. Yang, J. Shi, and L. Carbone, “TEASER : Fast and certifiable point cloud registration,” *IEEE Trans. Robot.*, vol. 32, no. 2, pp. 314–333, 2020.
- [35] T. Halsted and M. Schwager, “The Riemannian elevator for certifiable distance-based localization,” *Preprint*, 2022, Accessed: Dec. 18, 2022. [Online] Available: https://msl.stanford.edu/papers/halsted_reimannian_2022.pdf.
- [36] F. Marić, M. Giamou, A. W. Hall, S. Khoubyarian, I. Petrović, and J. Kelly, “Riemannian optimization for distance-geometric inverse kinematics,” *IEEE Trans. Robot.*, pp. 1–20, 2022.
- [37] D. Cifuentes, S. Agarwal, P. A. Parrilo, and R. R. Thomas, “On the local stability of semidefinite relaxations,” *Mathematical Programming*, no. 193, pp. 629–663, 2022.
- [38] C. Holmes and T. D. Barfoot, “An efficient global optimality certificate for landmark-based SLAM,” *arXiv:2206.12961*, Nov. 2022.
- [39] F. Dümbgen, C. Holmes, and T. D. Barfoot, “Safe and smooth: Certified continuous-time range-only localization,” *arXiv:2209.04266*, Dec. 2022.
- [40] A. N. Tikhonov and V. Y. Arsenin, “Solutions of ill-posed problems,” *SIAM Review*, vol. 21, no. 2, pp. 266–267, 1979.
- [41] G. H. Golub and C. F. Van Loan, *Matrix Computations*, 4th ed. The John Hopkins University Press, 2013.
- [42] L. Vandenberghe, “Chordal graphs and semidefinite optimization,” *Foundations and Trends in Optimization*, vol. 1, no. 4, pp. 241–433, 2015.
- [43] A. Goudar, W. Zhao, T. D. Barfoot, and A. P. Schoellig, “Gaussian variational inference with covariance constraints applied to range-only localization,” in *IEEE/RSJ IROS*, 2022.

APPENDIX

This appendix is published along with the *arXiv* verison of this paper and provides additional mathematical details and results.

A. Derivation of Dual Variables

We provide the detailed derivations for the computation of the optimal dual variables $\hat{\rho}$ and $\hat{\lambda}$, given a candidate solution \hat{f} . First, plugging in the expressions for \mathbf{Q} , \mathbf{A}_i ($i = 0 \dots N$), \mathbf{R} and \hat{f} in (13), we obtain

$$\begin{bmatrix} \hat{\lambda}_1 \hat{x}_1 \\ -\frac{\hat{\lambda}_1}{2} \\ \hat{\lambda}_2 \hat{x}_2 \\ -\frac{\hat{\lambda}_2}{2} \\ \vdots \\ \hat{\rho} - \sum_n \frac{\hat{\lambda}_n}{2} \|\hat{x}_n\|^2 \end{bmatrix} = \frac{1}{E} \begin{bmatrix} -2\mathbf{Y}_1 \Sigma_1^{-1} \mathbf{e}_1 \\ \mathbf{1}^\top \Sigma_1^{-1} \mathbf{e}_1 + \\ -2\mathbf{Y}_2 \Sigma_2^{-1} \mathbf{e}_2 \\ \mathbf{1}^\top \Sigma_2^{-1} \mathbf{e}_2 \\ \vdots \\ -\sum_n \mathbf{b}_n^\top \Sigma_n^{-1} \mathbf{e}_n \end{bmatrix}. \quad (34)$$

The N equations corresponding to the substitution variables take the form

$$(\forall n) \quad -\frac{1}{2} \hat{\lambda}_n = \frac{1}{E} \mathbf{1}^\top \Sigma_n^{-1} \mathbf{e}_n, \quad (35)$$

which can be solved for $\hat{\lambda}_n$. Plugging the solution into the other ND rows involving $\hat{\lambda}_n$, we need to show that

$$(\forall n) \quad \hat{x}_n \hat{\lambda}_n = -2 \frac{1}{E} \hat{x}_n \mathbf{1}^\top \Sigma_n^{-1} \mathbf{e}_n \stackrel{?}{=} -2 \frac{1}{E} \mathbf{Y}_n \Sigma_n^{-1} \mathbf{e}_n, \quad (36)$$

or in other words, we need these equations to be redundant. Because \hat{x}_n are stationary points of (2), we have

$$(\forall n) \quad \nabla_{\mathbf{x}_n} f = 4(\mathbf{Y}_n - \hat{x}_n \mathbf{1}^\top) \Sigma_n^{-1} \mathbf{e}_n = \mathbf{0}, \quad (37)$$

from which (36) follows trivially. Finally, we can use the last row of the linear system in (13) to solve for $\hat{\rho}$, which gives

$$\begin{aligned} \hat{\rho} &= \sum_n \left(\frac{\hat{\lambda}_n}{2} \|\hat{x}_n\|^2 - \frac{1}{E} \mathbf{b}_n^\top \Sigma_n^{-1} \mathbf{e}_n \right) \\ &= -\frac{1}{E} \sum_n \left(\|\hat{x}_n\|^2 \mathbf{1}^\top + \mathbf{b}_n^\top \right) \Sigma_n^{-1} \mathbf{e}_n \\ &= -\frac{1}{E} \sum_n \left(\mathbf{e}_n^\top - 2\hat{x}_n^\top \mathbf{Y}_n + 2\|\hat{x}_n\|^2 \mathbf{1}^\top \right) \Sigma_n^{-1} \mathbf{e}_n \\ &= -\frac{1}{E} \sum_n \mathbf{e}_n^\top \Sigma_n^{-1} \mathbf{e}_n - 2\hat{x}_n^\top (\mathbf{Y}_n - \hat{x}_n \mathbf{1}^\top) \Sigma_n^{-1} \mathbf{e}_n \\ &= -\frac{1}{E} \sum_n \mathbf{e}_n^\top \Sigma_n^{-1} \mathbf{e}_n. \end{aligned} \quad (38)$$

where we have substituted in $\hat{\lambda}_n$ in the first step, the definition of \mathbf{b}_n in the second step, and the stationarity condition (37) to yield the final expression.

1) *GP solution:* Building on the result from the previous section, we can derive the form of the optimal dual variables when we add a regularization term to the cost function. Starting from (29), we arrive at almost the same system of equations as before, but with additional rows for the new

dimensions in $\boldsymbol{\theta}$, and additional terms for the motion prior, added on the right-hand side:

$$\begin{bmatrix} \hat{\lambda}_1 \hat{x}_1 \\ \mathbf{0} \\ -\frac{\hat{\lambda}_1}{2} \\ \hat{\lambda}_2 \hat{x}_2 \\ \mathbf{0} \\ -\frac{\hat{\lambda}_2}{2} \\ \vdots \\ \hat{\rho} - \sum_n \frac{\hat{\lambda}_n}{2} \|\hat{x}_n\|^2 \end{bmatrix} = \frac{1}{E} \begin{bmatrix} -2\mathbf{Y}_1 \Sigma_1^{-1} \mathbf{e}_1 \\ \mathbf{0} \\ \mathbf{1}^\top \Sigma_1^{-1} \mathbf{e}_1 \\ -2\mathbf{Y}_2 \Sigma_2^{-1} \mathbf{e}_2 \\ \mathbf{0} \\ \mathbf{1}^\top \Sigma_2^{-1} \mathbf{e}_2 \\ \vdots \\ -\sum_n \mathbf{b}_n^\top \Sigma_n^{-1} \mathbf{e}_n \end{bmatrix} + \frac{1}{N} \begin{bmatrix} \mathbf{R}_{1,x} \hat{f} \\ \mathbf{R}_{1,v} \hat{f} \\ 0 \\ \mathbf{R}_{2,x} \hat{f} \\ \mathbf{R}_{2,v} \hat{f} \\ 0 \\ \vdots \\ 0 \end{bmatrix}.$$

$\mathbf{R}_{n,x}$ and $\mathbf{R}_{n,v}$ are the first D rows, and remaining rows, respectively, of \mathbf{R} as defined in (26).

Note that both the left-hand and right-hand sides do not change for the rows corresponding to the substitutions. Therefore, we can still use (35) to solve for $\hat{\lambda}$. The last step is to show that the remaining rows are redundant, which we show for the two example motion priors separately.

Example 1: For the zero-velocity prior, we have $\hat{\boldsymbol{\theta}} = \hat{\mathbf{x}}$ and the rows with $\mathbf{R}_{n,v}$ in (A1) vanish. Then, we only need to show that

$$(\forall n) \quad \hat{\boldsymbol{\theta}}_n \hat{\lambda}_n = \hat{\mathbf{x}}_n \hat{\lambda}_n \stackrel{?}{=} 2\mathbf{Y}_n \Sigma_n^{-1} \mathbf{e}_n + \frac{1}{N} \mathbf{R}_{n,x} \hat{\mathbf{x}}. \quad (39)$$

Equations (39) hold because $\hat{\boldsymbol{\theta}}_n$ are stationary points of the cost function $f(\boldsymbol{\theta}) + r(\boldsymbol{\theta})$ defined in (16), which means that

$$\mathbf{0} = \nabla_{\mathbf{x}_n} f(\hat{\boldsymbol{\theta}}) + \nabla_{\mathbf{x}_n} r(\hat{\boldsymbol{\theta}}) \quad (40)$$

$$= 4 \frac{1}{E} (\mathbf{Y}_n - \hat{\mathbf{x}}_n \mathbf{1}^\top) \Sigma_n^{-1} \mathbf{e}_n + 2 \frac{1}{N} \mathbf{R}_{n,x} \hat{\mathbf{x}}, \quad (41)$$

and (39) follows.

Example 2: For the constant-velocity motion prior, we need to show that

$$(\forall n) \quad \hat{\boldsymbol{\theta}}_n \hat{\lambda}_n = \begin{bmatrix} \hat{\mathbf{x}}_n \\ \hat{\mathbf{v}}_n \end{bmatrix} \hat{\lambda}_n \stackrel{?}{=} \begin{bmatrix} 2\mathbf{Y}_n \Sigma_n^{-1} \mathbf{e}_n \\ \mathbf{0} \end{bmatrix} + \begin{bmatrix} \mathbf{R}_{n,x} \\ \mathbf{R}_{n,v} \end{bmatrix} \hat{\boldsymbol{\theta}}. \quad (42)$$

As for the first example, the first D rows of system (42) hold because $\hat{\boldsymbol{\theta}}_n$ are stationary points with respect to \mathbf{x}_n , so (41) must hold. For the last D rows, we have

$$\mathbf{0} = \nabla_{\mathbf{v}_n} r(\hat{\boldsymbol{\theta}}) = \frac{1}{N} \mathbf{R}_{n,v} \hat{\boldsymbol{\theta}}, \quad (43)$$

which confirms that the additional equations are satisfied. Finally, we start with the same expression for $\hat{\rho}$ as in the second-last row of (38), but this time, using (43), we obtain

$$\begin{aligned} \hat{\rho} &= -\frac{1}{E} \sum_n \mathbf{e}_n^\top \Sigma_n^{-1} \mathbf{e}_n - 2\hat{x}_n^\top (\mathbf{Y}_n - \hat{x}_n \mathbf{1}^\top) \Sigma_n^{-1} \mathbf{e}_n \\ &= -\frac{1}{E} \sum_n \mathbf{e}_n^\top \Sigma_n^{-1} \mathbf{e}_n - \frac{1}{N} \sum_n \hat{x}_n^\top \mathbf{R}_{n,x} \hat{\boldsymbol{\theta}} \\ &= -\frac{1}{E} \sum_n \mathbf{e}_n^\top \Sigma_n^{-1} \mathbf{e}_n - \frac{1}{N} \sum_n \hat{x}_n^\top \mathbf{R}_{n,x} \hat{\boldsymbol{\theta}} - \hat{\mathbf{v}}_n^\top \mathbf{R}_{n,v} \hat{\boldsymbol{\theta}} \\ &= -\frac{1}{E} \sum_n \mathbf{e}_n^\top \Sigma_n^{-1} \mathbf{e}_n - \frac{1}{N} \hat{\boldsymbol{\theta}}^\top \mathbf{R} \hat{\boldsymbol{\theta}}, \end{aligned} \quad (44)$$

where we have used (41) for the second line. From there, we add $\sum_n \hat{\mathbf{v}}_n^\top \mathbf{R}_{n,v} \hat{\boldsymbol{\theta}}$, which is zero because of (43), to make the relationship with the quadratic cost function more evident.

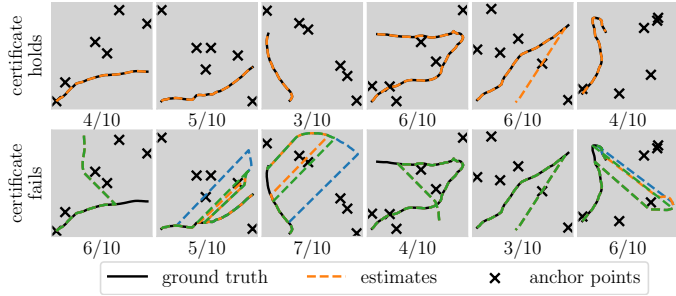


Fig. 7: Visualization of optimal (top) and suboptimal (bottom) solutions found by a local GN solver in range-only continuous-time localization, in simulation. Each column corresponds to a different random setup. Solid black lines correspond to ground truth trajectories and the dashed coloured lines correspond to estimates from various random initializations. Out of 100 random setups, the 6 shown setups yield, for a high proportion of random initializations (see labels below each plot), suboptimal solutions. The proposed method allows to identify such suboptimal solutions with little additional computational cost.

B. Simulation results

In Figure 7, we study the simulated setups prone to yield local optima. We fix the noise level to $\sigma_d = 10^{-3}$ and show the results for the constant-velocity prior. A qualitative analysis suggests that, whenever the anchors are sufficiently spread, meaning they are not almost co-linear (or almost co-planar in the three-dimensional case), the local solver converges to the global minimum. Indeed, for the shown 6 out of 100 random setups, which are the only ones consistently leading to local minima, the anchors are close to co-linear. The local optima, shown in the second row of Figure 7, are partially mirrored versions of the optimal solution, around the line defined by the anchors. For each setup, we show three local solutions in dashed lines of different colors. The proportion of local and global solutions, respectively, is shown below each plot. At this noise level, the certificate correctly labels all optimal solutions, and fails for all local solutions. As noted in Section IV-A, this suggests that strong duality holds and that the certificate is sufficient *and* necessary, for this noise level.